Article   🔒 Full Access

Deuterium Rotating Frame NMR Relaxation Measurements in the Solid State under Static Conditions for Quantification of Dynamics

Prof. Liliya Vugmeyster ✉, Dr. Dmitry Ostrovsky

Find it @FSU

Abstract

The feasibility of static deuterium rotating frame NMR relaxation measurements for characterization of slow timescale motions in powder systems is demonstrated. Using a model compound dimethyl sulfone-d_6, we show that these measurements yield conformational exchange rates and activation energy values in accordance with results obtained with other techniques. Furthermore, we demonstrate that the full Liouvillian approach as opposed to the Redfield approximation is necessary to analyze the experimental data.

1 Introduction

Rotating frame relaxation measurements in the solid-state ($R_{1\rho}$) have recently gained momentum as powerful techniques for studies of biomolecular dynamics.[1-9] These studies have been performed at ^{15}N and ^{13}C nuclei and utilized magic-angle spinning (MAS) for site-specific resolution. With the technical advances of fast magic-angle spinning approaches and current spinning speeds exceeding 100 kHz,[10-12] it now becomes feasible to consider

utilizing deuterium nuclei, which are known to be very sensitive dynamics probe.[13, 14] The effective quadrupolar coupling constant of methyl group undergoing fast rotations is arc

[13] One of the earlier classic works considering the behavior of ^2H nuclei under rotating frame conditions was written by Vega at al. in regards to considering cross-polarization of spin 1/2 and spin 1 nuclei, however the effects of motions were not included in the treatment.[15]

Before turning to developing ^2H methods under MAS condition, it is important to understand the details of ^2H dynamics in the rotating frame under static conditions. Furthermore, the static experiments are expected to be a useful tool for selectively labeled protein samples for which it is difficult to obtain site-specific resolution, such as varieties of amorphous biological aggregates and fibrils, in particular amyloids. Advantages of static conditions also include simplification in the analysis of the data, as physical rotations introduce additional time-dependence of the interactions and can cause complications when the time scales of motions are close to the spinning frequencies.[6,16, 17]

While multiple static ^2H methods for studies of dynamics have been developed from 1970's,[13,18-27] examples of ^2H $R_{1\rho}$ measurements in the literature are surprisingly sparse, and is likely due to the complicated behavior of powder samples under rotating frame conditions. Reported studies utilized single crystals to partially simplify this problem.[20] With the modern computational methods, a full treatment of $R_{1\rho}$ relaxation is achievable.

The goal of this work is to demonstrate the feasibility of static deuterium $R_{1\rho}$ experiments to probe slow time scale motions. We use a standard sample, dimethyl-sulfone-d_6 (DMS) that has been a model system for the development of static ^2H methods as well as MAS $R_{1\rho}$ ^{13}C methods.[4,6] DMS methyl groups undergo a two-site exchange corresponding to a 180° flip around the molecule C_2 axis (Figure 1) and thus determination of the rate of flips can serve as a probe of sensitivity of the method. Additionally, the usual methyl 3-site jumps motions of the methyl groups are present. They occur on a much faster time scale and have been extensively studied by other methods, in particular ^2H longitudinal relaxation.[28, 29] Some of these studies also suggested the presence of additional motional modes,[28] which can likely be attributed to small-angle fluctuations within local potential minima.
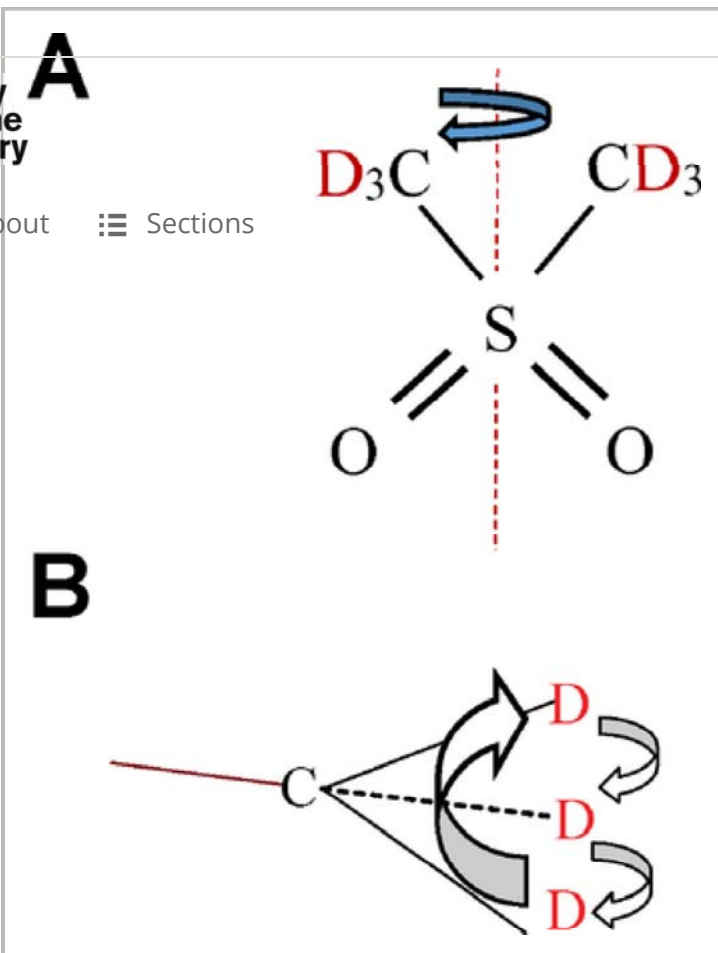
Figure 1

Open in figure viewer | PowerPoint

Structure of dimethyl-sulfone-d_6 (DMS) highlighting the motional modes of A) the 180° flipping motion around the C_2 axis and B) fast 3-site methyl jumps.

We show that static deuterium $R_{1\rho}$ relaxation measurement coupled with computational modeling provide dynamics information on this flip rate, with the values consistent with what has been found using other techniques. We also provide the basic framework of the theory as well as data collection and treatment for this experiment.

2 Theory

2.1 Review of General Formalism of Spin 1 Relaxation in Rotating Frame in Redfield Limit

Density matrix for the spin-1 system can be written in the basis of the following operators [Eq. (1)] (Vega [1]:

$$\widehat{S}_x = \frac{1}{2}\begin{pmatrix} 0 & 1 & 0 \\ 1 & 0 & 1 \\ 0 & 1 & 0 \end{pmatrix}, \ \widehat{S}_y = \frac{1}{2}\begin{pmatrix} 0 & -i & 0 \\ i & 0 & -i \\ 0 & i & 0 \end{pmatrix},$$ (1)

$$\widehat{J}_x = \frac{1}{2}\begin{pmatrix} 0 & -i & 0 \\ i & 0 & i \\ 0 & -i & 0 \end{pmatrix}, \ \widehat{J}_y = \frac{1}{2}\begin{pmatrix} 0 & 1 & 0 \\ 1 & 0 & -1 \\ 0 & -1 & 0 \end{pmatrix}$$

$$\widehat{S}_z = \frac{1}{\sqrt{2}}\begin{pmatrix} 1 & 0 & 0 \\ 0 & 0 & 0 \\ 0 & 0 & -1 \end{pmatrix}, \ \widehat{J}_z = \frac{1}{\sqrt{2}}\begin{pmatrix} 0 & 0 & -i \\ 0 & 0 & 0 \\ i & 0 & 0 \end{pmatrix},$$

$$\widehat{Q} = \frac{1}{\sqrt{6}}\begin{pmatrix} 1 & 0 & 0 \\ 0 & -2 & 0 \\ 0 & 0 & 1 \end{pmatrix}, \ \widehat{K} = \frac{1}{\sqrt{2}}\begin{pmatrix} 0 & 0 & 1 \\ 0 & 0 & 0 \\ 1 & 0 & 0 \end{pmatrix}$$

They obey the following normalization condition tr($O_k^+O_l$)=δ_{kl}. Hamiltonian for the spin-1 system associated with the deuteron nucleus under rotating frame relaxation consists of terms related to interaction with the static magnetic field, quadrupole interaction with the electric field gradient, and the RF spin-lock field. In the rotating frame, the part of the Hamiltonian associated with the static magnetic field disappears, the spin-lock field term remains constant and its contribution to the Hamiltonian is $\sqrt{2}\omega_{sl}\widehat{S}_x$ while the quadrupole interaction can be separated into the constant secular part $\sqrt{\frac{2}{3}}\omega_q\widehat{Q}$ and fluctuating part due to internal molecular motions.[13]

We will first review previous results summarized by Maarel[20] for a ^{2}H single crystallite under the spin-lock interaction in the Redfield limit.[30] We will show how the treatment can be extended toward the full Liouvillian approach to account for deviations caused by the Redfield approximation. Further, we will extend the treatment to the static powder conditions.

Under the combined action of the spin-lock and quadrupole fields the components of the density matrix interconvert within two separate sets of 4 components, $\{\widehat{S}_x, \widehat{J}_x, \widehat{K}, \widehat{Q}\}$ and $\{\widehat{S}_y, \widehat{J}_y, \widehat{S}_z, \widehat{J}_z\}$. For the first set, the master equation is given by Equation (2).[20] Note, we will not reproduce all the equations here and refer the reader to the cited work. Maarel uses a different basis, which corresponds to the basis used here as: $\widehat{T}_{20} = \widehat{Q}$, $\widehat{T}_{11}(a) = \widehat{S}_x$, $\widehat{T}_{21}(s) = i\widehat{J}_x$, $\widehat{T}_{22}(s) = \widehat{K}$, $\widehat{T}_{10} = \widehat{S}_z$, $\widehat{T}_{11}(s) = -i\widehat{S}_y$, $\widehat{T}_{21}(a) = -\widehat{J}_y$, $\widehat{T}_{22}(a) = -i\widehat{J}_z$

$$\frac{d}{dt}\begin{pmatrix} S_x \\ J_x \\ K \\ Q \end{pmatrix} = \begin{pmatrix} -r_1 & -\omega_q & 0 & 0 \\ \omega_q & -r_2 & -\omega_{sl} & -\sqrt{3}\omega_{sl} \\ r_5 & \omega_{sl} & -r_3 & 0 \\ \sqrt{3}r_5 & \sqrt{3}\omega_{sl} & 0 & -r_4 \end{pmatrix}\begin{pmatrix} S_x \\ J_x \\ K \\ Q \end{pmatrix}$$ (2)

We use the same symbols for the coefficients of components of the density matrix as for the operators themselves, but without hats. The *r* terms in Equation (2) represent relaxation

contributions calculated in the Redfield approximation. The relaxation rates are as follows [Eq. 3]:

$$r_1 = \frac{3}{2} \frac{\omega_q^2 J_0(0) + 4\omega_{sl}^2 J_0(\omega_1)}{\omega_1^2} + \frac{5}{2} J_1(\omega_L) + J_2(2\omega_L)$$

$$r_2 = \frac{3}{2} \frac{\omega_q^2 J_0(0) + 4\omega_{sl}^2 J_0(\omega_1)}{\omega_1^2} + \frac{1}{2} J_1(\omega_L) + J_2(2\omega_L)$$

$$r_3 = J_1(\omega_L) + J_2(2\omega_L) \tag{3}$$

$$r_4 = 3J_1(\omega_L)$$

$$r_5 = \frac{3}{2} \frac{\omega_q \omega_{sl} [J_0(0) - J_0(\omega_1)]}{\omega_1^2}$$

where ω_L is Larmor frequency, $\omega_1^2 = \omega_q^2 + 4\omega_{sl}^2$ and J_0, J_1, and J_2 are the usual spectral density functions.[31] The evolution of the second set of 4 components $\{\hat{S}_y, \hat{J}_y, \hat{S}_z, \hat{J}_z\}$ can be described by similar equations.

2.2 Limitations of Redfield Theory and the Necessity of Liouvillian Approach

The validity of the Redfield approximation is based on the assumption that the relaxation rate is significantly smaller than the rate of motions that cause it.[30] This assumption can be easily verified for relaxation rates given by $J_1(\omega_L)$ and $J_2(2\omega_L)$. An order of magnitude estimate of J_1 caused by a motion with rate k is given by Equation 4:[13]

$$J_1(\omega_L) \propto \frac{\omega_q^2 k}{\omega_L^2 + k^2} \tag{4}$$

$J_1(\omega_L) \ll k$ because $\frac{\omega_q^2}{\omega_L^2 + k^2} < \left(\frac{\omega_q}{\omega_L}\right)^2 \ll 1$. Of course, J_1 can be even smaller than the estimate of Eq. 4 for small-angle motions. The same argument applies to $J_2(2\omega_L)$.

The contributions to the relaxation originating from the secular terms at frequencies much smaller than Larmor frequency (i.e, J_0 in Redfield limit), do not necessarily satisfy the conditions of the Redfield theory. The sufficient condition would be [Eq. 5]:

$$J_0(0) \propto \frac{\omega_q^2}{k} \ll k \rightarrow k \gg \omega_q \tag{5}$$

which doesn't always hold. Note that for the large angle motions this becomes the necessary condition as well.

For slow motions, $k < \omega_q$, the Redfield theory becomes unjustified, and thus one must employ the more general Liouvillian approach. In the Liouvillian approach, the spin density matrix retains explicit dependence on the spatial coordinates. We consider the case where orientations of the deuteron bond inside the molecule (and, therefore, orientations of the principal axes system of the quadrupole interaction) occupy well-defined discrete positions connected by instantaneous jumps. In this approximation, the spatial dependence of the density matrix is represented by a vector consisting of density matrices in each of the individual geometric orientations that the deuteron occupies during its motion.

Because relaxation due to transitions between different Zeeman levels satisfies the requirements of the Redfield theory, it is possible to treat the respective terms in the Hamiltonian to the second order of time-dependent perturbation theory, which leads to the relaxation terms given by J_1 and J_2 as in the evolution matrix of Eqs. (2) and (3). The relaxation which does not involve the exchange between different Zeeman levels arises because of the differences in the values of ω_q for different sites. If we define [Eq. 6]:

$$\rho_i = \begin{pmatrix} S_x \\ J_x \\ K \\ Q \end{pmatrix} \tag{6}$$

for the components of the density matrix for a site i then the Liouville equation can be written in the block form as Equation 7:

$$\frac{d}{dt}\begin{pmatrix} \rho_1 \\ \rho_2 \\ \vdots \\ \rho_n \end{pmatrix} = \begin{pmatrix} A_1 + K_{11} & K_{12} & \cdots & K_{1n} \\ K_{21} & A_2 + K_{22} & \cdots & K_{2n} \\ \vdots & \vdots & \ddots & \vdots \\ K_{n1} & K_{n2} & \cdots & A_n + K_{nn} \end{pmatrix}\begin{pmatrix} \rho_1 \\ \rho_2 \\ \vdots \\ \rho_n \end{pmatrix} \tag{7}$$

where the diagonal blocks A_i are the same as in Eq. (2), but with contributions from J_0 removed and with site-dependent values of ω_q. The off-diagonal blocks represent exchange between the sites and are given by $K_{ij} = k_{ij}I$, where I is the identity matrix; the diagonal blocks $K_{ii} = -\sum_{j \neq i} K_{ji}$ provide conservation of probability.

We note that comparison between Redfield and Liouvillian approaches has been recently performed for ^{1}H $R_{1\rho}$ relaxation under MAS conditions.[9] It has been concluded that Redfield treatment is adequate for small-angle fluctuations and spinning speeds far from the rotary resonance conditions, while for other cases the Liouvillian treatment is necessary.

2.3 Qualitative Descriptions of Coherent and Incoherent Contributions to Evolution

In order to gain a qualitative insight into the behavior of coherent (oscillating) and non-coherent contributions into the relaxation it is convenient to consider the limit in which t relaxation terms in Eq. (2) are small compared to the coherent terms. In this case relaxation does not change the eigenvector basis, given by Equations 8:

$$\frac{2\omega_{sl}}{\omega_1}\widehat{S}_z + \frac{\omega_q}{2\omega_1}\left(\widehat{K} + \sqrt{3}\widehat{Q}\right),\ 0$$

$$\frac{\sqrt{3}}{2}\widehat{K} - \frac{1}{2}\widehat{Q},\ 0 \tag{8}$$

$$\frac{\omega_q}{\sqrt{2}\omega_1}\widehat{S}_z \pm \frac{i}{\sqrt{2}}\widehat{J}_x - \frac{\omega_{sl}}{\sqrt{2}\omega_1}\left(\widehat{K} + \sqrt{3}\widehat{Q}\right),\ \pm i\omega_1$$

where the second quantity in each line shows the eigenvalue in the absence of relaxation.[20] The last two eigenvectors correspond to terms oscillating with frequency ω_1. For solid powder samples the frequency ω_1 is not a single value due to different crystallite orientations. Additional factors affecting ω_1 is the presence of large scale jumps with rates on the order of magnitude or smaller than ω_q. The complexity of oscillations caused by variability in ω_1 is hard to disentangle from the relaxation of these eigenvectors. We therefore focus only on the two non-oscillating eigenvectors, $\frac{2\omega_{sl}}{\omega_1}\widehat{S}_z + \frac{\omega_q}{2\omega_1}\left(\widehat{K} + \sqrt{3}\widehat{Q}\right)$, and $\frac{\sqrt{3}}{2}\widehat{K} - \frac{1}{2}\widehat{Q}$. Relaxation changes the eigenvalues of Eq. (8). Zero eigenvalues remain real (i. e., eigenvectors remain non-oscillating), but become negative. The separation of eigenvalues into 2 real and 2 complex, with the imaginary part given approximately by ω_1, persists even when more complicated Eq. (7) is used and when the assumption of the small relaxation contribution does not hold.

2.4 Distribution of Real Eigenvalues and the Two-Exponential Approximation to Relaxation Decay Curves

We will now describe the distribution of the relaxation rates corresponding to real eigenvalues (i. e., corresponding to non-oscillating eigenvectors), for Equations (2) and (7) obtained by numerical simulations. For powdered samples, relaxation rates depend on ω_q (and in the case of J_0 explicitly so) and thus contribute to relaxation anisotropy. In general the effect of anisotropy is very complex and it is not possible to pinpoint a one to one correspondence between the molecular orientation and powder pattern frequencies.[13] In the following discussion we will focus on the region around the major singularities of the powder pattern (horns). In the absence of motions on the order of C_q, the major contributions originate from crystallites at 90° angle of the largest component of the effective quadrupolar tensor with respect to the magnetic field.

To arrive at the distribution of the relaxation rates in a powder sample for the horns frequency, the following procedure is used. Each crystallite orientation is rated by how m[...]sional is contributing to the intensity at the horns' frequencies. Next, the non-oscillating eigenvalues are selected and their contributions to the $\hat{S}_x$ operator are multiplied (weighted) by the contribution of the selected crystallite orientation to the overall intensity at the horns frequencies. We thus arrive at a set of eigenvalues and their weights which can be summarized by an eigenvalue density plots, such as in Figure 2. In this example we have chosen a two-mode motion corresponding to 3-site jumps and large angle flips mode for DMS at 73 °C.
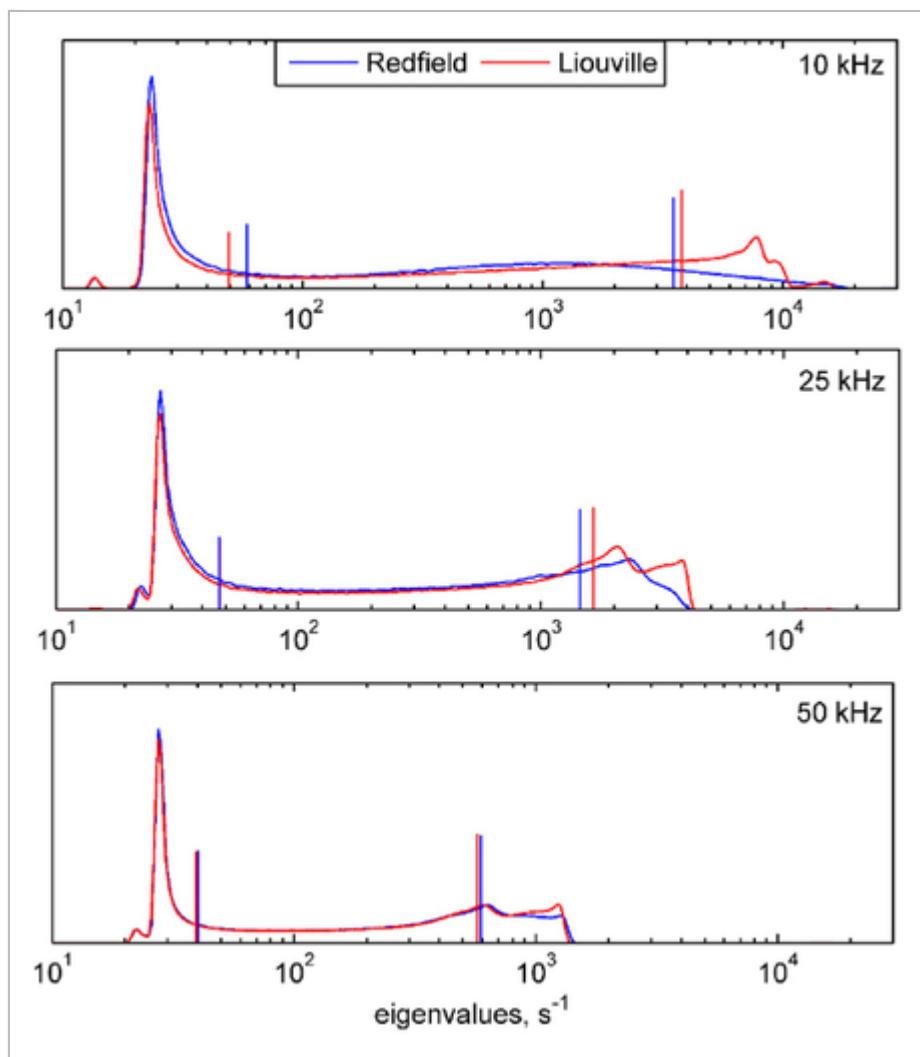
Figure 2

Theoretical distribution of eigenvalues (density) corresponding to two motional modes in DMS: 3-site jumps with the rate constant of 4.9×10^9 s^{-1} and two-site flips of 180° flip around the molecule C_2 axis of DMS with the rate constant of 8000 s^{-1}. Simulations were performed according to Redfield (blue) and Liouville (red) approaches at three values of spin-lock field of 10 kHz, 25 kHz, and 50 kHz.

Magnetization decay curves were simulated for 100 delays between 2 μs and 50 ms. Vertical lines represent the relaxation rate constants obtained from the two-exponential fit. The height of the lines reflects relative fractions of the two components. Number of tiles used was 100 000 for the distribution curves and 1600 for the magnetization decay curves. All data are shown for the horn positions of the powder-pattern spectrum.

As can be seen from the plots, the eigenvalues cover a wide range of about 3.5 orders of magnitude. The lower end is given by fast 3-site jumps while the upper limit is due to contribution of the slow flips. Importantly, the distribution tends to be bimodal, emphasizing contributions from the two different motional modes. Further, for the large eigenvalues, there is a considerable deviation between the Redfield and Liouvillian calculations, indicating that motions are outside of the validity of the Redfield theory. The deviations are more apparent for the lower spin-lock field strengths. The Liouvillian approach has a larger density of higher-value eigenvalues, corresponding to faster relaxation. Further, if the oscillating component to the relaxation are included (Figure 3), it is evident that oscillations persist for longer times in the relaxation decay curves for the Redfield theory in comparison to the Liouvillian approach.
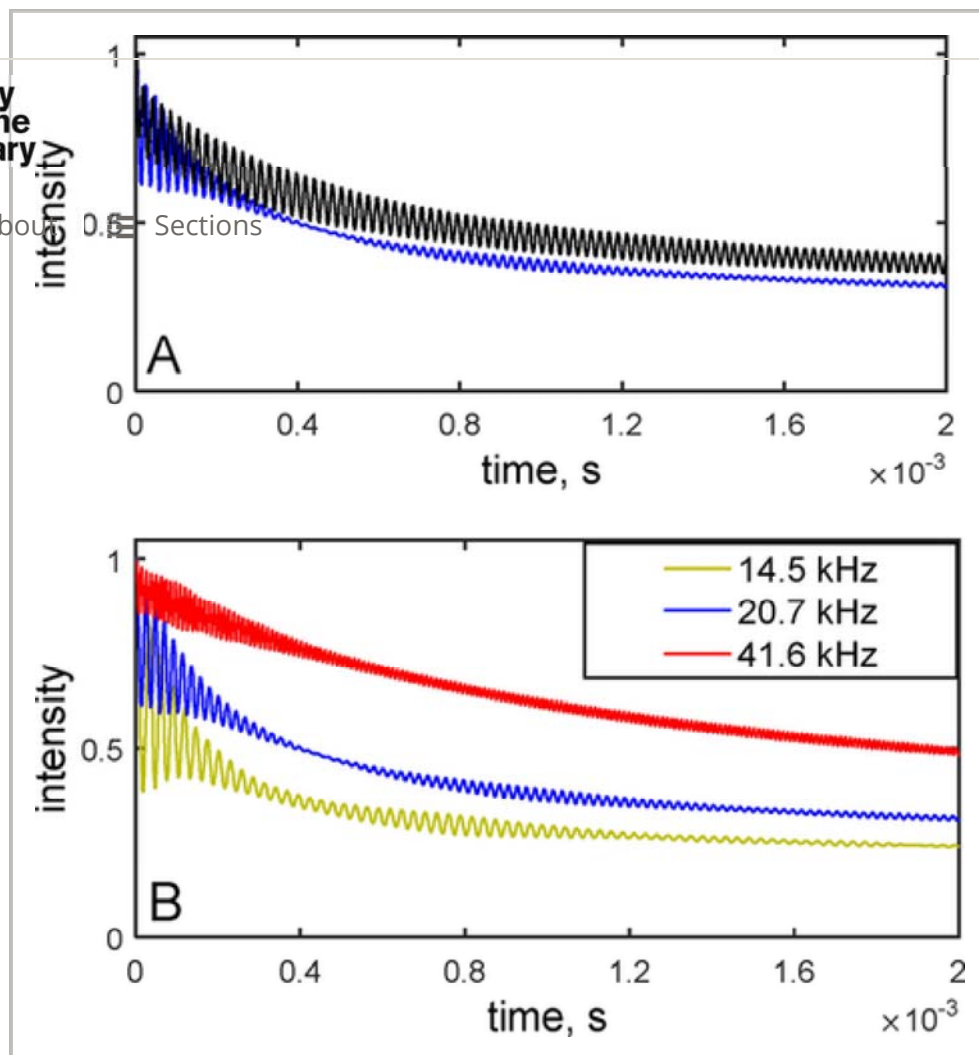
Figure 3

Simulated magnetization decay curves according to A) the Redfield (black) and Liouvillian (blue) approaches with the spin-lock field of 20.7 kHz and B) Liouvillian approach for three spin-lock fields strength of 14.5, 20.7 and 41.6 kHz. Peak intensities are taken at horn positions and are normalized to initial values. Two motional modes are included: 3-site jumps with the rate constant of 4.9×10^9 s^{-1} and two-site flips of 180° flip around the molecule C_2 axis of DMS with the rate constant of 8000 s^{-1}.

Though the true distribution of the eigenvalues is continuous, we found it sufficient to model the resulting decay curves with the two-exponential function. Fitting the decay curves with more parameters leads to unstable values of the fitted parameters without producing any more insight. The location of vertical lines in Figure 2 represent the fitted relaxation rates according to the two-exponential model with the use of 100 relaxation delays to sample the decay curve. They provide a visual representation of the fitted relaxation rates

and underlying eigenvalue densities. The experimental results are treated within the same framework.

3 Results and Discussion

$R_{1\rho}$ measurements have been performed using the pulse sequence depicted in Figure 4, which utilizes a heat-compensation block to ensure a constant total spin-lock time throughout all relaxation delays and is conceptually analogous to the pulse sequences presented by Vega for half-integer quadrupolar spins,[17] which has also been utilized by Wimperis and co-workers.[32] The details are presented in the Experimental Section.
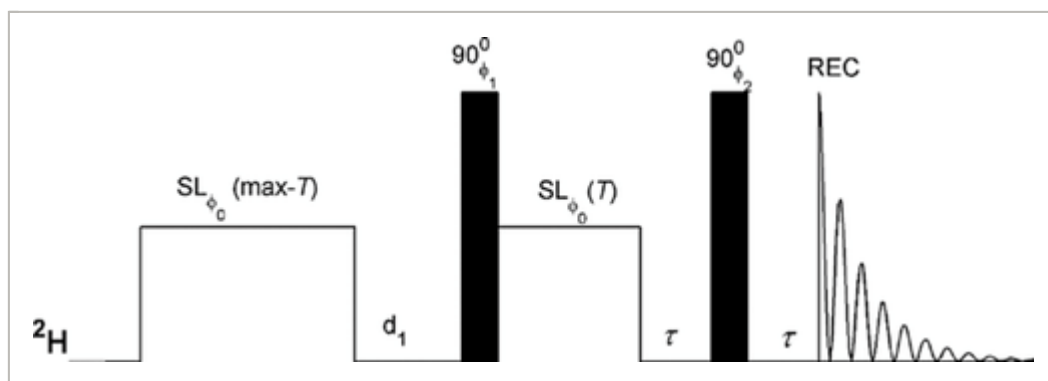
Figure 4

Open in figure viewer | PowerPoint

Pulse sequence for static ^2H solid-state $R_{1\rho}$ measurements. Heat compensation block SL(max-T) is followed by the inter-scan delay d_1 and the preparation 90° pulse, followed by a variable spin lock delay SL(T). The detection is accomplished using the quadrupole echo scheme, τ −90°− τ. Phase cycle corresponds to: $\varphi_0=x$; $\varphi_1=-y,y$; $\varphi_2=-x,x$; receiver=$-y,y$. The duration of d_1 varied between 1 and 4.5 s for the maintenance of constant temperature. Spin-lock field strength varied between 14.5 and 41.6 kHz with the durations SL(T) between 10 µs and 50 ms.

Static quadrupole echo detection scheme (τ−90°−τ block in Figure 4) in principle permits for data analysis at each individual frequency of the powder pattern. In this study we do not investigate the effect of relaxation anisotropy and consider the relaxation behavior only around the major singularities of the powder pattern, corresponding primarily to the 90° orientation of each S−C bond vector with respect to the magnetic field. The DMS sample contained residual amount of water, as can be seen from the narrow center peak in the quadrupole echo lineshape (Figure 5, top panel), which is due to the HOD signal. Water incorporation did not affect longitudinal relaxation times at the horns (major singularities) positions. Water can have some effect on the flipping motion in DMS, especially if relaxation is monitored around the zero frequency.[29] Representative spectra of DMS from the $R_{1\rho}$

measurements are shown in Figure 5. The relaxation rates were obtained for the regions of ±0.5 kHz around the horn positions. Taking a narrow range of frequencies rather than focusing on one point of the powder pattern permits to account for any drift/distortions in the exact frequency values of the horns and improves the overall quality of the signal.
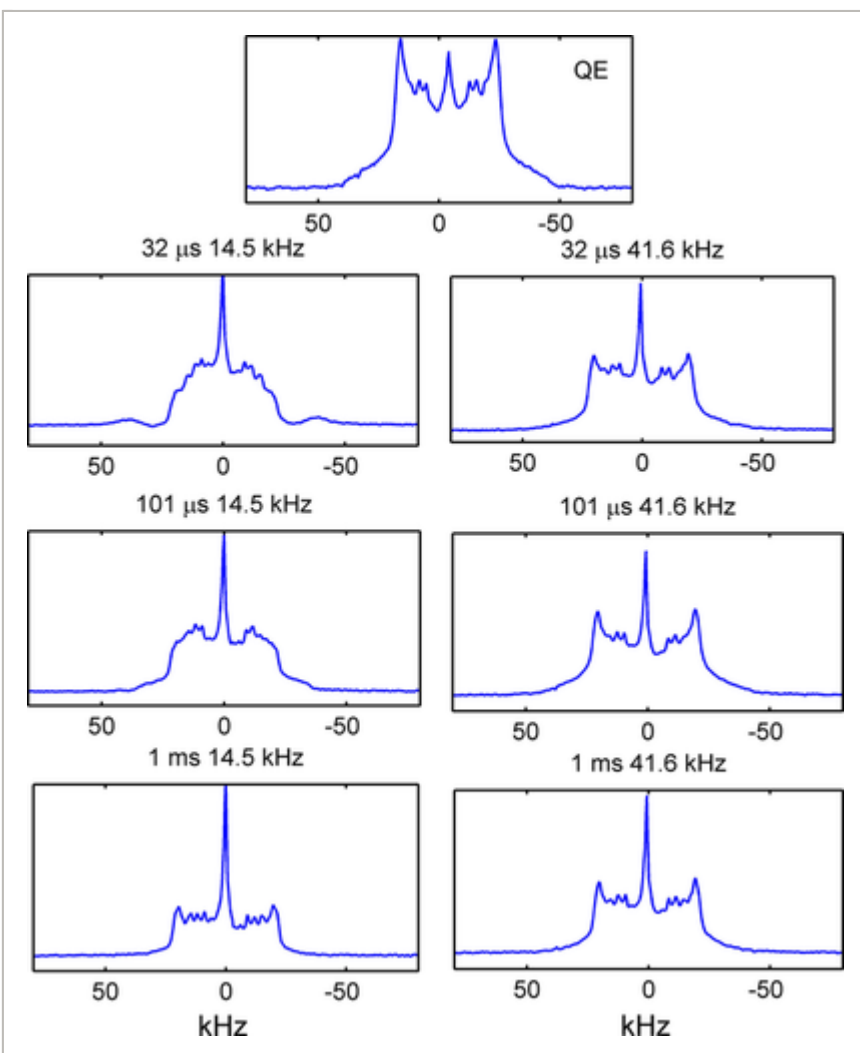
Figure 5

Open in figure viewer │ PowerPoint

^{2}H partially relaxed spectra of DMS at 73 °C under $R_{1\rho}$ conditions with spin-lock field strength and relaxation delay times indicated at each panel, collected using the pulse sequence of Figure 2 Top center panel: quadrupole echo lineshape at 73 °C.

3.1 Relaxation Data Treatment using a Two-Exponential Approximation

As follows from the theoretical section, the easiest way to analyze the data is to invoke the two-exponential approximation to the decay curves at each field. This yields a crude estimate of the slow and fast relaxing components of the S_x operator (Figure 2). Further, the main approach for simulations that are performed to fit the experimental results was based on the Liouvillian treatment. Throughout the text we will indicate when Redfield treatment is used to demonstrate the discrepancies between the two approaches. Additionally, as the fast relaxing component is most sensitive to the flipping motions, we will focus on presenting the data and analysis for this component.

There is an obvious trade-off between incorporation of small relaxation delays into sampling of the magnetization decay curves (Figure 6) in order to better capture the fast relaxing component and the fact that oscillations in S_x are most pronounced for smaller times. A reasonable solution is to keep the smallest relaxation delays in the 100−300 μs region. In addition, selecting the same delays in the simulations as were chosen in experiment compensates for the systematic errors from the cut-off and provides a largely unbiased estimate of the flip rate.
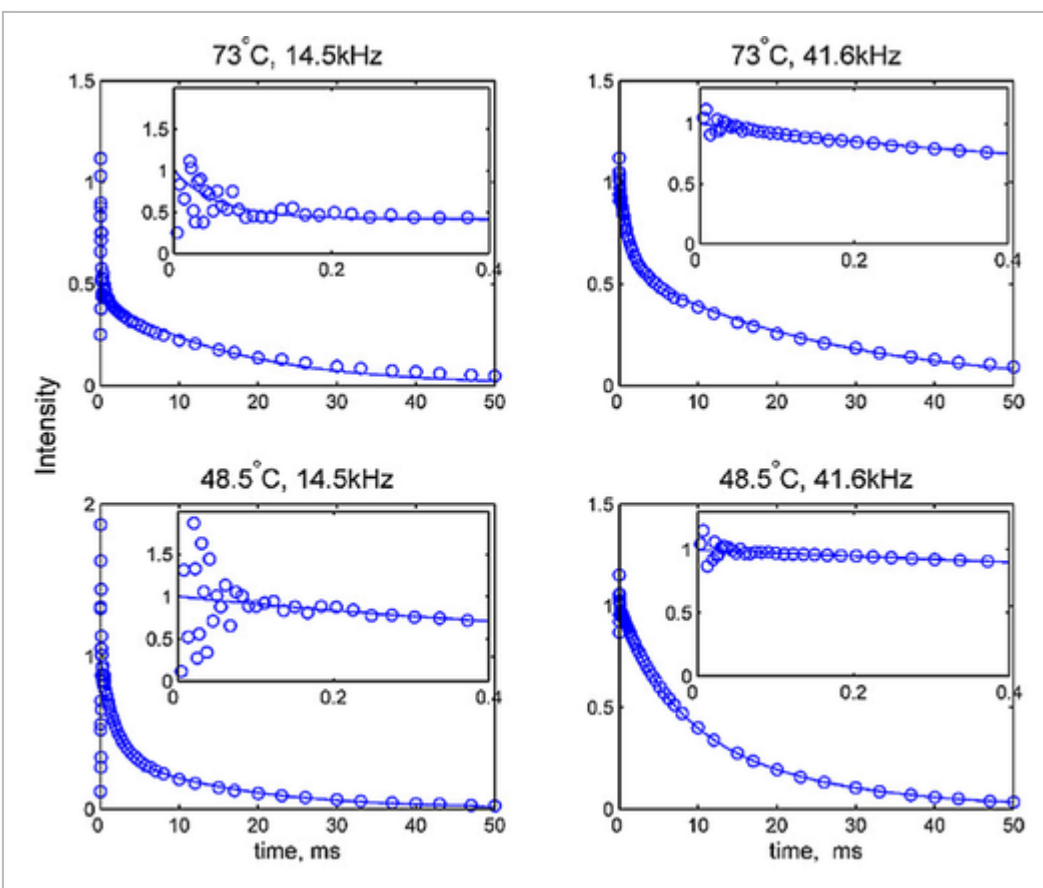
Figure 6

Open in figure viewer │ PowerPoint

Examples of experimental magnetization decay curves at 73 and 48.5 °C and the
spin-lock field strengths of 14.5 and 41.6 KHz, for the horn positions of the
powder pattern. The solid lines correspond to the two exponential fit. The inserts
highlight the initial decay region. The intensities are normalized to the value
predicted by two-exponential fit at $t=0$.

What is striking however, is that for simulations the extent of distortion in the magnetization decay curves due presence of oscillations is considerably higher than what is observed in the experimental data. This indicates that some additional averaging of the oscillations is happening in the experiment due to presence of B_1 inhomogeneity. To partially account for this effect, simulations for each spin-lock field strengths were performed with ±5 % range from the central value and the simulated curves were averaged over this range (Supporting Information SI1).

The noise in resulting relaxation dispersion profiles with this treatment is relatively high (Figure 7), however it is still possible to see some tendency for deviations between the Liouvillian and Redfield approaches for low temperatures, as demonstrated in Figure 8 for data at 48.5 °C. The fitted value of flip rate with Redfield approach is 1200 ± 400 s^{-1}, while it is 880 ± 90 s^{-1} with Liouvillian approach. The quality of the fit according to the Redfield formalism is somewhat worse compared to the Liouvillian approach.
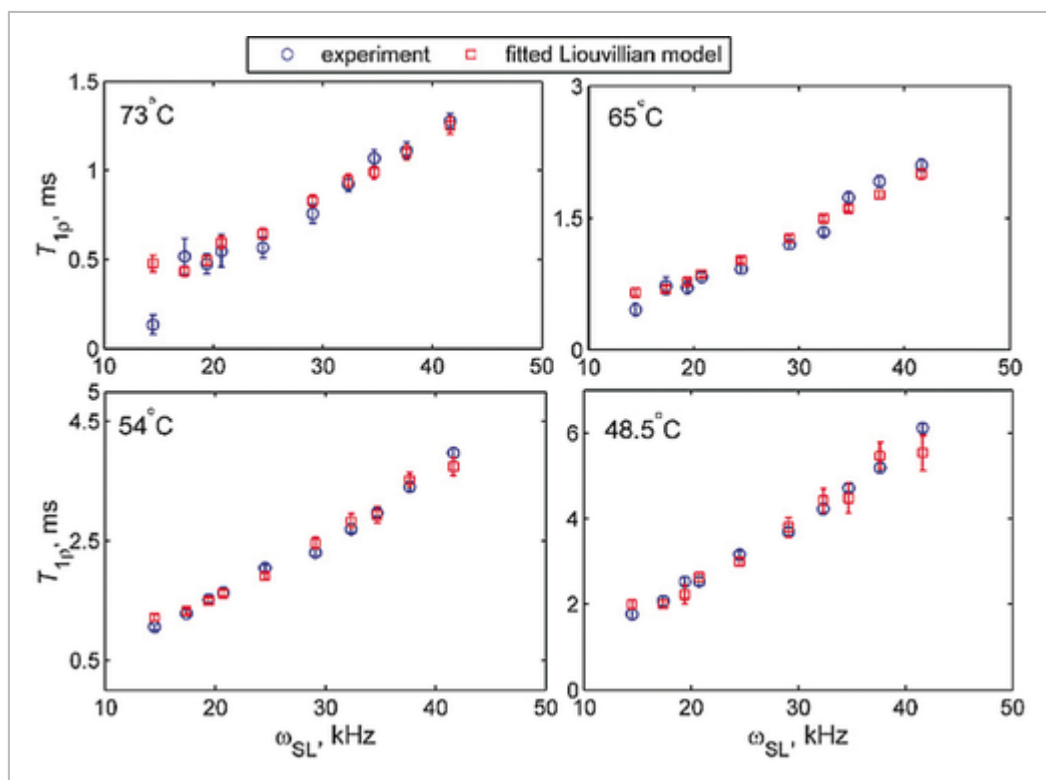
Figure 7

Relaxation dispersion profiles for the fast relaxing component, $T_{1\rho}$ versus ω_{SL}. Experimental results from the two-exponential approximation (blue circles) and the best-fit simulation according to the Liouvillian approach (red squares) with the inclusion of ±5 % averaging due to B_1 inhomegenuity. Data corresponds to the horn positions of the powder pattern. For 73 and 65 °C only the delays longer than 100 µs were included in the analysis, and for 54 and 48.5 °C only the delays longer 300 µs.
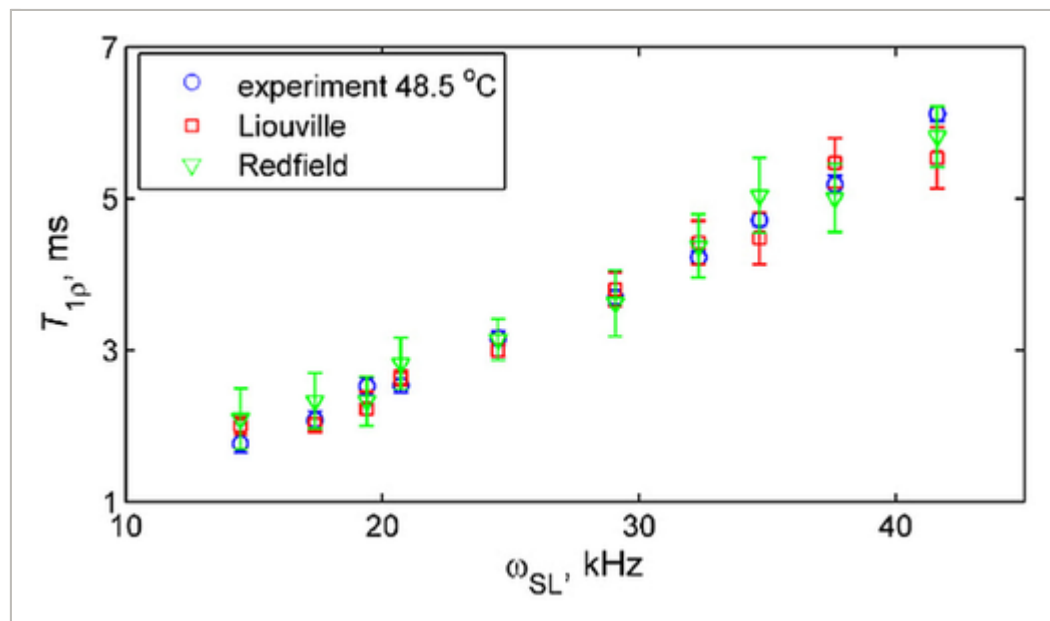
Figure 8

Experimental relaxation dispersion profiles at 48.5 °C for the fast component of the two-exponential fits (blue circles) compared with the simulations based on the Redfield approach with the best-fit flip rate of 1200 s⁻¹ (green triangles) and Liouvillian approach with the best-fit flip rate of 880 s⁻¹ (red squares). Simulations include ±5 % averaging for inclusion of B_1 inhomegenuity factor and all data corresponds to the horn positions.

Despite the high level of noise, the treatment retains sensitivity to the main motional parameter of interest – flip rate. The best fitted values of the flip rates resulting from comparison of experimental relaxation dispersion profiles of the fast component to simulations with Liouvillian treatment are shown in Figure 9 for the 73–48.5 °C range and the sensitivity of the fits to the flip rates is demonstrated in SI2. The slow-relaxing component is considerably less sensitive to the values of the flip rate (SI3), as expected, because it is dominated by $J_1(\omega_L)$ and $J_2(2\omega_L)$ spectral densities, as shown in Eq. (3). Both the

values of the flip rates k_{flip} and the activation energy value obtained from the temperature dependence under the assumption of Arrhenius behavior (Figure 9) are well within the values reported in the literature for DMS.[6,29,33-35] Our fitted value of the activation energy E_a is 79±2 kJ/mol. The literature range is 60–91 kJ/mol, and specifically the value obtained by ¹³C MAS $R_{1\rho}$ relaxation is 72±3 kJ/mol.[6] It is also known that line shape analysis can underestimate the value of E_a due to temperature-dependence of the static (i. e., those not induced by motions) contributions to the line-width, thus in our case the best comparison is with another rotating frame relaxation measurement approach. Our fitted value of the prefactor is ln$A$ is 36.4±0.7, with the literature range of 29 to 41. The comparison with the values of the prefactors is less reliable in general, as they are strongly dependent on the width of the temperature range used in the studies.[29,36] Nevertheless, our value is in good agreement with ln$A$ of 33.6±1.0 obtained from the ¹³C MAS $R_{1\rho}$ relaxation measurements.[6] Thus, we conclude that even with this crude treatment the experiment yields correct values of the flip rates.
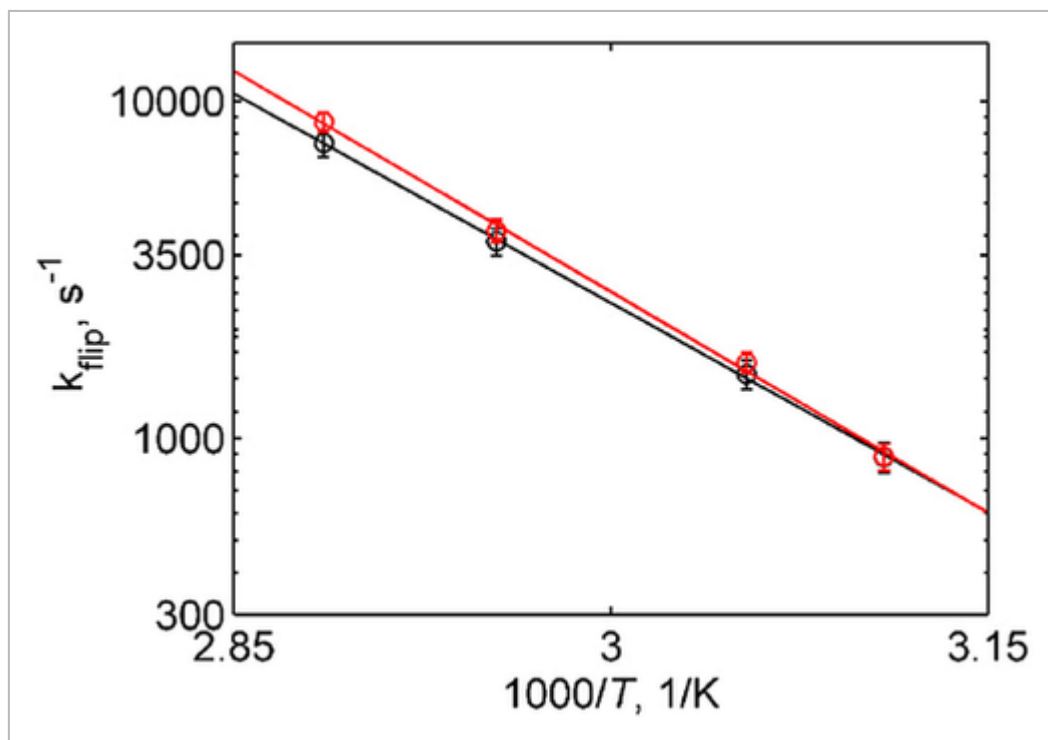
Figure 9

Open in figure viewer | PowerPoint

Semilog plot of k_{flip} versus $1/T$ corresponding to 73–48.5 °C temperature range for fits performed with the two-exponential function without the removal of the oscillatory component (black) and with the removal of the oscillatory components for low spin-lock field strengths (red). Solid lines represent the linear fit to the data: E_a=79±2 kJ/mol, ln$A$=36.4±0.7 (black), E_a=83±3 kJ/mol, ln$A$=37.8±1.0 (red).

3.2 Limit of the Technique

At 40 °C the decay curves for spin-lock fields of 29 kHz and higher approach mono-exponentiality (Fig SI4), while for lower fields some deviations from mono-exponentiality is still apparent. Thus, the flipping motion at this temperature is close to the limit of sensitivity of this technique. The value of k_{flip} for this temperature can be estimated as 300 s^{-1} using mon-exponential fits for all fields. This value is in good agreement with the projection from the Arrhenius fit.

At 5 °C the decay curves for all fields are mono-exponential, indicating that the flipping motion is effectively frozen and does not contribute to $J(0)$. When simulations are performed with the inclusion of only the 3-site jumps mechanism (with the 3-site jump rate constant fixed from the T_1 experiment), there is a reasonable agreement between the simulated and experimental results. (Figure 10). The slight deviation can be attributed to small-angle fluctuations of the methyl axis. For example, when an additional mode of 5° –amplitude two-site jumps with the rate constant of 5.5×10^8 s^{-1} is included, the agreement becomes almost perfect. We note that this mechanism does not affect the rotating frame relaxation at high temperatures in the presence of the much more effective flipping motion; additionally, the small angle fluctuations are expected to be faster at higher temperatures which will further lower their contributions to the $T_{1\rho}$ relaxation. A hint of these additional motions was seen by Cutnell and Venable,[28] who analyzed non-exponentiality in ^{2}H T$_{1z}$ decay curves of polycrystalline DMS in a very broad temperature range between −90 to +73 °C. An alternative explanation of the slight discrepancies between the experimental data at 5 °C and simulations which take into account only the 3-site jumps mechanism is the residual contribution of the flipping motion. If the Arrhenius dependence of k_{flip} is projected to 5 °C, it is expected to lie below 10 s^{-1} and will not have any effect on the R$_{1\rho}$ relaxation. If we assume that the Arrhenius dependence is not followed, the rate constant of about 100 s^{-1} can match $T_{1\rho}$ times at the spin-lock fields of 20–30 kHz, but the dependence on the spin-lock frequency cannot be reproduced.
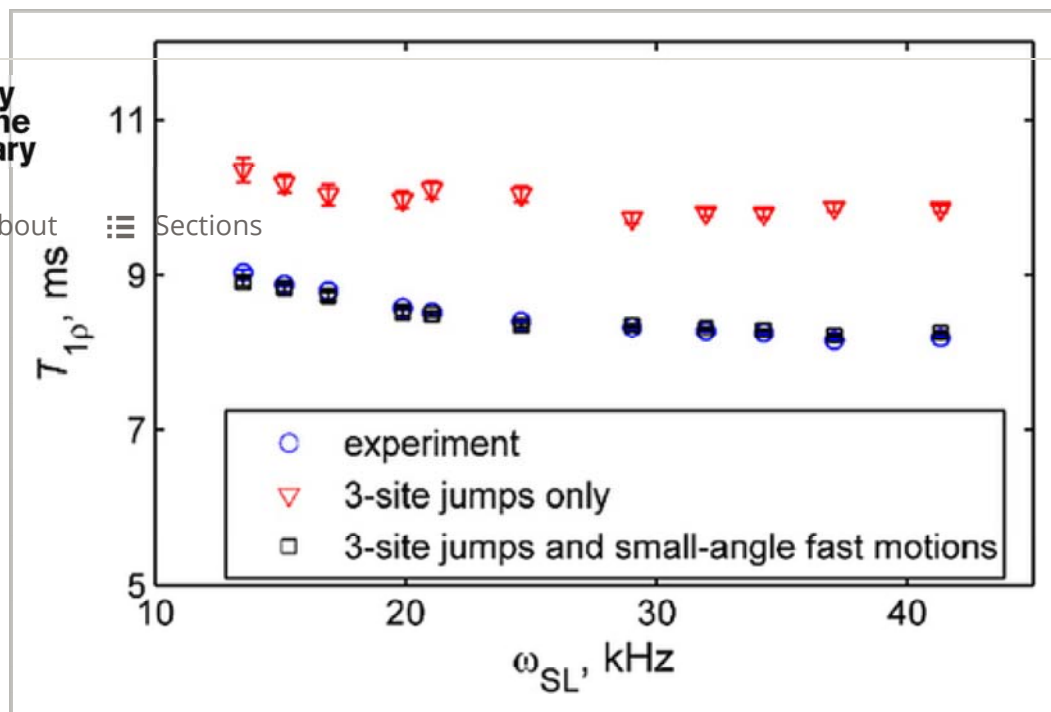
Figure 10

Open in figure viewer │ PowerPoint

Relaxation dispersion profile for 5 °C: experiment (blue circles), simulations with the inclusion of the methyl 3-site jumps rate constant of 1.2×10^9 s^{-1} determined from T_1 measurements (red triangles), simulations with the inclusion of both the 3-site jump mechanism and additional mode of small angle fluctuations (black squares): 2-site jumps with 5° amplitude and 5.5×10^8 s^{-1} rate constant.

3.3 Data Treatment with Removal of Coherent Oscillations Demonstrates the Importance of Full Liouvillian Calculations

Removal of the oscillatory coherent component by explicitly taking into account the frequency ω_1 requires a detailed data for short delays below 100 μs and a somewhat involved analysis explained in detail in SI5. The oscillations are most pronounced at lower fields, as can be seen from the approximation of Eq. (8). The non-oscillatory component of $\hat{S}_x$ is given by $\frac{2\omega_{sl}}{\sqrt{\omega_q^2 + 4\omega_{sl}^2}}$ and increases with the increase in spin-lock frequency ω_{sl}, while the oscillatory component given by $\frac{\omega_q}{\sqrt{\omega_q^2 + 4\omega_{sl}^2}}$ decreases, and therefore overall effect of the increase in the spin-lock field is to decrease the amplitude of the oscillations (see also Figure 3B). Note, the approximation of Eq. (8) is based on the Redfield treatment and simulations based on the Liouvillian treatment (Figure 3A) show the same trend as well as demonstrate the slower rate of decay of the oscillatory component for lower spin-lock field frequencies.

Thus, detailed data below 100 μs were collected for the fields in 14–21 kHz range (first four fields) in the dispersion curves in order to trace these oscillatory effects. The resulting experimental and simulated decay curves now yield the fast decay times with much smaller error bars, which permits for a more quantitative comparison for the discrepancies with Redfield and Liouvillian treatments. Indeed, as can be seen from Figure 11, for the Redfield-based simulations even for the best-fit value of the flip rate the whole dispersion profile cannot be reproduced at 73 °C – the simulations yield the wrong slope. This indicates that the limit of Eq. (5) is reached. In addition, Redfield-based simulations yield distinctly different best-fit values of the flip rate compared to the Liouvillian approach. Examples in Figure 11 demonstrate that the fitted values of flip rates differ by 38 % at 73 °C and 48 % for 48.5 °C between the Redfield and Liouvillian treatments.
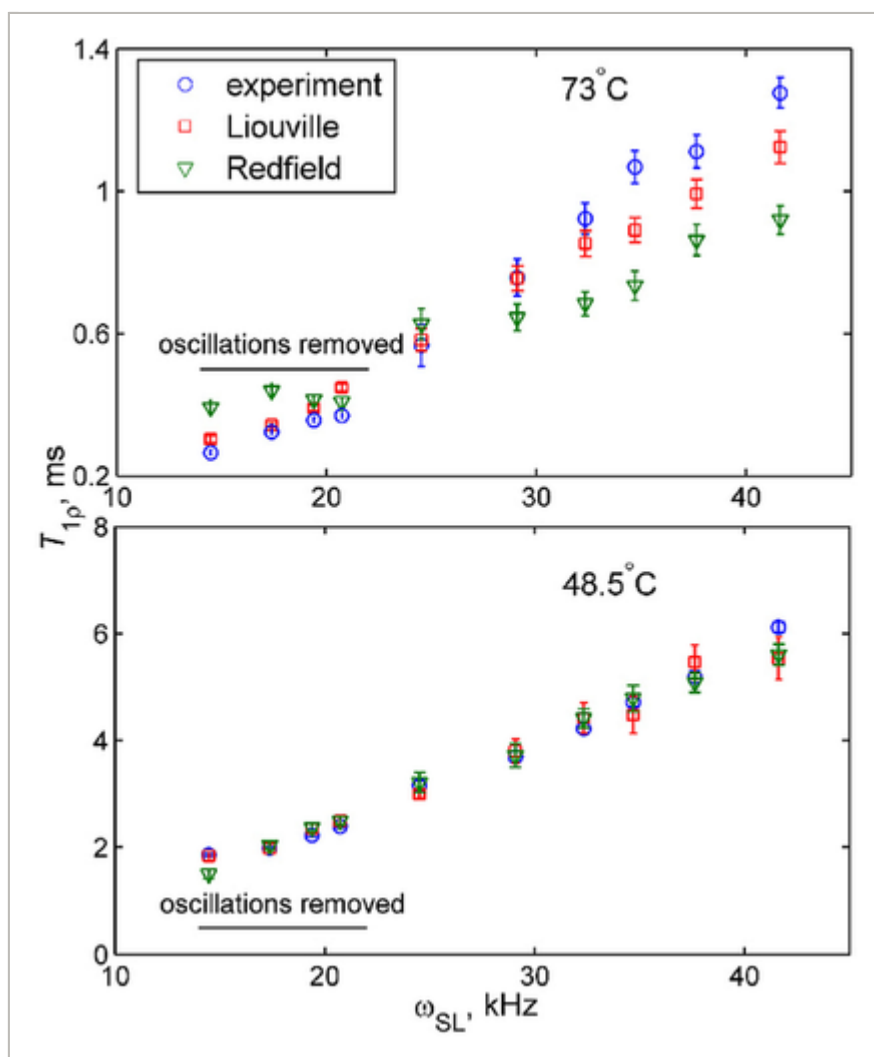
Figure 11

Open in figure viewer | PowerPoint

Experimental dispersion profiles at 73 and 48.5 °C for the fast component of the two-exponential fits (blue circles) are compared with the best-fit simulations from the Redfield (green triangles) and Liouville approaches (red squares). For the four

lowest spin-lock fields the oscillatory component was removed as described in SI5. The following best-fit flip rates were used: 12,000 s⁻¹ with Redfield and 8700 s⁻¹ with Liouvillian for 73 °C, and 1700 s⁻¹ with Redfield and 880 s⁻¹ with Liouvillian for 48.5 °C. Simulations include ±5 % averaging for inclusion of B_1 inhomegenuity factor. χ^2 values for the fits are given in SI6.

Removing the oscillatory component in the full Liouvillian treatment of the data slightly changes the fitted values of the flip rate constants in comparison to the crude approach described in the previous section (Figure 9). Overall, the fitted flip rates with and without oscillatory components are within the error bars, as well as the resulting value of the activation energy, which is 79±2 kJ/mol without the removal of the oscillatory component and 83±3 kJ/mol when the removal is performed.

3.4 Discussion Regarding Applicability to Biological Samples

An important question is whether this methodology can be applied to biological samples with much lower sensitivity than DMS. In this regard, it is important that the crude treatment that does not require experimental determination of coherent oscillations is still sensitive to the motional process. For estimates of the motional constants it can be sufficient to perform measurement at three to four values of the spin-locking field rather than sampling the whole profile and constrain sampling of decay curves to about 10—15 delays, which further increases feasibility of the technique for lower sensitivity samples. The choice of the values of spin-lock fields would be governed by a compromise between the following factors: lower fields provide a better separation between the fast and slow relaxing component (Figure 2) and induce less sample heating, while higher fields lead to an enhanced signal and are less impacted by the oscillations (Figure 3B) Minimal expected signal to noise requirements are about 40 for the shortest delay in the relaxation series for the major singularities and expected measurement times are 5 to 8 days for an entire relaxation dispersion profile. Qualitatively, the results will be similar if one integrates the entire powder pattern as opposed to evaluating the intensities at the horn positions. If the horns are well-defined in the spectrum, it is best to focus on these singularities as they provide a minimal mixture of crystallite orientation dependence.[13] Additionally, if the signal quality is high, it is possible to assess relaxation anisotropy which can provide further insights into motional mechanisms. Motional narrowing of the line shape can significantly reduce effective quadrupolar coupling constant. If the narrowing is substantial (i. e., the presence of large-angle motions faster than ω_q), it may be sufficient to integrate the whole line shape for the analysis. Further, if the motions are in the fast regime with respect to ω_q, then oscillatory component is largely suppressed and the Redfield limit of Eq. (5) is likely to hold, which also leads to more familiar relaxation dispersion profiles seen for ¹³C and ¹⁵N nuclei. This regime can hold for very flexible regions of the proteins such as loops in globular proteins and intrinsically disordered

regions of functional amyloids. We expect the methodology to be especially valuable for the assessment of the dynamics in these disordered regions in combination with selective/si te labelling approaches.

In principle, the detection block can be modified to include multiple-echo acquisition scheme for sensitivity enhancement purpose.[37], [38] Further, extensions of this approach for measurements under MAS conditions are possible but require a substantially different theoretical treatment due to additional time-dependence of the Hamiltonian and the possibility of interference between motions, coupling constants, and the physical rotation.[6,16]

4 Conclusions

Using DMS-d$_6$ as a model compound, we have demonstrated feasibility of static deuterium $R_{1\rho}$ relaxation measurements for determination of slow motion rate constants in powder samples. Relaxation dispersion profiles were obtained under spin-locking fields ranging between 14 to 42 kHz. We discussed data treatment using a simple two-exponential approximation to the decay curves and a more sophisticated treatment that explicitly takes into account coherent oscillations. Both yield very similar results in regards to the conformational exchange rate. The values of rate constants and activation energies are well within the range reported for DMS by other techniques.

Additionally, we discussed the limits of validity of the Redfield theory as opposed to the full Liouvillian approach for the data analysis. The latter is necessary for the description of the experimental data in DMS for which the motional regime is such that the rate constant is slower than the quadrupolar coupling interaction constant. This work builds foundation for the extension of deuterium $R_{1\rho}$ relaxation measurements toward biological samples at static conditions as well as potentially at magic-angle spinning conditions.

Materials and Methods

Experimental

DMS has been purchased from Cambridge Isotopes Laboratories, Inc. (MA) and packed into a 5 mm glass tube in the amount of 48 mg.

The R$_{1\rho}$ experiment according to the pulse sequence in Figure 2 is performed with the quadrupolar echo scheme using a two-step phase cycle. The calibration of the spin-lock field strength was performed using a similar pulse sequence in which the spin lock period was followed by a nutation pulse with a 90° phase shift. The duration of this pulse was varied, and the zero-crossing of the signal is observed when the nutation corresponds to the π/2 pulse.

All experiments were performed on a 600 MHz NMR spectrometer with a Bruker Avance I console using a wide-line low-E probe[39] with a 5-mm inner diameter coil built at the National High Magnetic Field Laboratory.[39] Quadrupolar echo τ_{echo} delay was set to 31 μs. 90° hard power pulses corresponded to 2 μs. Spin lock times varied between 10 μs and 50 ms and powers varied from 14.5 to 41.6 kHz. The general strategy was to collect approximately 65 relaxation delays for each of the 9–10 spin-lock fields. For the determination of the fast coherent oscillatory component as well as rapidly relaxing components of the decay, large number of delays below 500 μs was included. At 5 °C the sampling of decay curves started at 1 ms with 35 relaxation delays. 16–32 dummy scans were utilized. Spectra were processed with 0.5 kHz line broadening.

Set point temperature calibrations were performed with lead nitrate[40] and using D_2O as a reference point. To maintain constant temperature throughout the experiment it is the necessity to equalize the amount of heating due to variable RF and spin-lock time. Within the same spin lock field strength measurements, the heat compensation block ensures the same amount of heating throughout all delays. However, it is somewhat harder to account for variations in heating with the variable spin-lock strength. Our approach was to use an internal thermometer based on the T_1 values in the presence of a "dummy" spin-lock heat compensation block. T_1 values of DMS are very sensitive to temperature in this temperature range and corrections in effective sample temperatures can be made by varying the recycle delay in such a manner that the same T_1 values are obtained with the dummy spin-lock field at all spin-lock field strengths. Of course, it is possible to almost entirely get rid of this effect by setting the recycle delay for a very light duty cycle, which in our case would results in the values of over 6 sec. Thus, this approach was impractical and instead all recycle delays were calibrated to match the heating at the intermediate value of spin lock field of 22 kHz with the recycle delay of 2 s at this field. The spread in recycle delay values was thus from 1 s at the lowest field to 4.5 s at the highest field. The temperature correction was obtained by matching T_1 values in the presence of spin-lock to the T_1 data in the absence of spin-lock using interpolation according to the Arrhenius Law. The corrections are on the order of 2–3 degrees under the chosen conditions and the temperatures shown in all graphs account for this correction.

Computational Modeling

Modeling of the $R_{1\rho}$ experiment can be divided into the following steps: generating transverse coherence, evolution period in the presence of the rotating transverse field, and detection. We produced an idealized first step that creates a pure S_x coherence and used a spin-lock field in x direction of the rotating frame. Because we work with the full set of spin-1 coherences [Eq. (1)], it is not difficult to introduce various imperfections such as the effect of a finite pulse width, but it was unnecessary for our purposes. The detection block was

modeled with the inclusion of the quadrupole echo scheme, as was done in the experiment. All simulations were performed in Matlab and utilized blocks from the EXPRESS program designed primarily for simulations of ^{2}H line shapes and relaxation experiments of single coherences in Redfield limit.[41] In particular, the detection block involving quadropole echo scheme with the powder-averaging procedure and appropriate Eurler's angle transformations were taken from this program.

Evolution in the presence of the spin-lock field were considered either in the Redfield approximation or with the full Liouvillian treatment. In Redfield theory, the motions are considered fast enough (much faster than the typical relaxation rates) such that for each molecular orientation one can describe the spin state with a single vector of coherences. This vector is then subjected to the evolution matrix. The matrix elements of this 8×8 evolution matrix are obtained as the weighted average values for the matrix elements given in Eq. (2) (see also Maarel[20] Equations (16) and (17)) for all sites representing instantaneous orientations of the C−D bond vector. The elements of the evolution matrix are also dependent on the overall orientation of the molecule in the laboratory frame. To model the dependence on the relaxation delay, the initial vector of coherences is then transformed by the matrix exponent of the evolution matrix multiplied by the delay time.

The detection block is described in great detail in Vold et al.[41] The following is a brief summary. As there is no spin-lock in the detection period, we can select the coherence that will be detected (S_+) and consider it independently of the other coherences, which renders a significant computational simplification. During the detection period a typical time increment (dwell time) might be smaller than the typical time of exchange and therefore the simulation must include individual contributions of all sites into S_+. The evolution matrix during detection then consists of local frequencies w_q in each site for the diagonal terms and exchange rates for the off-diagonal terms of Eq. (7). The obtained signal is summed up over the orientations of the molecule in the lab frame according to one of several summation schemes.[41]

For the simulations based on the Liouvillian approach in the rotating frame, the state of the spin system is given by the 8×N dimensional vector combining the coherences in all sites. The evolution matrix is given by Eq. (7). All other details of implementation of the evolution and detection blocks are similar to those described in the above paragraph.

The simulation parameters were set up in the nested frames scheme which consisted of a total of 6 deuterium sites, split into the three sites of the methyl group with the ideal tetrahedral geometry (frame 1) nested within two sites connected by the π-flip of the DMS symmetry plane (frame 2) with the angle of 106° between the two S−C bond directions. The values of the 3-site jumps rate constants were fixed to those that reproduced experimental T_1 values at each temperature. The quadrupole constant was set to C_q=166.4 kHz, based on

the spectrum at 5 °C. For the powder averaging ZCW tiling algorithm[41] was used with 1600 tiles, which was found to be the minimum necessary for stable calculations. For simulation theoretical eigenvalues distributions profiles of Figure 2 100,000 tiles were used. The calculations in Redfield approximation were very fast and for Liouvillian method each $R_{1\rho}$ time delay required about 5 seconds on Intel Core i5 2.4 GHz CPU.

Acknowledgements

Conflict of interest

The authors declare no conflict of interest.

Supporting Information ⌄

References ⌄

Wiley Online Library

About   **Sections**